Molecular Neurobiology

Characterization of the mitochondrial aerobic metabolism in the pre- and perisynaptic districts of the SOD1G93A mouse model of amyotrophic lateral sclerosis

--Manuscript Draft--

Manuscript Number:	
Article Type:	Original Article
Keywords:	amyotrophic lateral sclerosis; SOD1G93A mouse; oxidative phosphorylation; synaptosomes; gliosomes.
Corresponding Author:	Giambattista Bonanno, Ph.D. University of Genova ITALY
First Author:	Silvia Ravera
Order of Authors:	Silvia Ravera
	Tiziana Bonifacino
	Martina Bartolucci
	Marco Milanese
	Elena Gallia
	Francesca Provenzano
	Katia Cortese
	Isabella Panfoli
	Giambattista Bonanno, Ph.D.
Abstract:	Amyotrophic lateral sclerosis (ALS) is an adult-onset fatal neurodegenerative disease characterized by muscle wasting, weakness and spasticity, due to a progressive degeneration of cortical, brainstem and spinal motor neurons, whose causes are still largely obscure, although astrocytes surely play a role in neuronal damage. Several mechanisms have been proposed to concur to ALS neurodegeneration, including mitochondrial dysfunction. We have previously shown profound modification of glutamate release and presynaptic plasticity in the spinal cord of mice expressing mutant SOD1G93A, a model of ALS. In this work, for the first time, we characterized the aerobic metabolism in two specific compartments actively involved in neurotransmission, i.e. the pre-synaptic district, using purified synaptosomes, and the perisynaptic astrocyte processes, using purified gliosomes, in SOD1G93A mice at different stages of the disease. ATP/AMP ratio appeared lower than controls in synaptosomes isolated from spinal cord, but not from other brain areas of SOD1G93A mice. Such energy impairment was linked to altered oxidative phosphorylation (OxPhos) and increment of lipid peroxidation. These metabolic dysfunctions were present during disease progression, starting at the very pre-symptomatic stages and did not depend on a different number of mitochondria or a different expression of OxPhos proteins in SOD1G93A mice synaptosomes. Conversely, gliosomes showed altered ATP/AMP ratio, only at the late stages of the disease, and increment of oxidative stress, although it did not display a significant decrement in the OxPhos activity. Data suggest that the presynaptic neuronal moiety plays a pivotal role in the energy metabolism dysfunction. Changes in the perisynaptic compartment seem subordinated to the neuronal damage.

Characterization of the mitochondrial aerobic metabolism in the pre- and perisynaptic districts of the *SOD1*^{G93A} mouse model of amyotrophic lateral sclerosis

Silvia Ravera[a,1], Tiziana Bonifacino[a,1], Martina Bartolucci[b], Marco Milanese[a,c], Elena Gallia[a], Francesca Provenzano[a], Katia Cortese[d], Isabella Panfoli[b,1], Giambattista Bonanno[a,c,1,*]

[1] Equally contributed.

[a] Department of Pharmacy, Unit of Pharmacology and Toxicology, University of Genoa, 16148 Genoa, Italy

[b] Department of Pharmacy, Laboratory of Biochemistry, University of Genoa, 16132 Genoa, Italy

[c] Center of Excellence for Biomedical Research, University of Genoa, 16132 Genoa, Italy

[d] Department of Experimental Medicine, Human Anatomy, University of Genoa, 16132 Genoa, Italy.

*Corresponding Author:

Prof. Giambattista Bonanno

E-mail: bonanno@difar.unige.it

Phone: +39 010 353 2658

ORCID codes:

Silvia Ravera: 0000-0002-0803-1042

Isabella Panfoli: 0000-0002-6261-1128

Giambattista Bonanno: 0000-0003-3744-5786

ABSTRACT

Amyotrophic lateral sclerosis (ALS) is an adult-onset fatal neurodegenerative disease characterized by muscle wasting, weakness and spasticity, due to a progressive degeneration of cortical, brainstem and spinal motor neurons, whose causes are still largely obscure, although astrocytes surely play a role in neuronal damage. Several mechanisms have been proposed to concur to ALS neurodegeneration, including mitochondrial dysfunction. We have previously shown profound modification of glutamate release and presynaptic plasticity in the spinal cord of mice expressing mutant *SOD1*^{G93A}, a model of ALS. In this work, for the first time, we characterized the aerobic metabolism in two specific compartments actively involved in neurotransmission, i.e. the pre-synaptic district, using purified synaptosomes, and the perisynaptic astrocyte processes, using purified gliosomes, in *SOD1*^{G93A} mice at different stages of the disease.

ATP/AMP ratio appeared lower than controls in synaptosomes isolated from spinal cord, but not from other brain areas of *SOD1*^{G93A} mice. Such energy impairment was linked to altered oxidative phosphorylation (OxPhos) and increment of lipid peroxidation. These metabolic dysfunctions were present during disease progression, starting at the very pre-symptomatic stages and did not depend on a different number of mitochondria or a different expression of OxPhos proteins in *SOD1*^{G93A} mice synaptosomes. Conversely, gliosomes showed altered ATP/AMP ratio, only at the late stages of the disease, and increment of oxidative stress, although it did not display a significant decrement in the OxPhos activity. Data suggest that the presynaptic neuronal moiety plays a pivotal role in the energy metabolism dysfunction. Changes in the perisynaptic compartment seem subordinated to the neuronal damage.

Keywords:

amyotrophic lateral sclerosis; SOD1^{G93A} mouse; oxidative phosphorylation; synaptosomes; gliosomes.

INTRODUCTION

Amyotrophic lateral sclerosis (ALS) is an adult-onset fatal neurodegenerative disease characterized by a progressive degeneration of cortical, brainstem and spinal motor neurons (MNs) leading to muscle wasting, weakness and spasticity [1, 2]. In the ALS patients, death essentially occurs because of respiratory failure, usually within three to five years after diagnosis [3, 4]. To date, no cure is available for ALS and the only FDA approved drugs are riluzole, that increases survival in patients of a few months with no evidence for amelioration of the quality of life [5], and edaravone, that was only very recently approved by the FDA and demonstrated to be active only with people who suffer from early-stage ALS [6].

ALS occurs in two different forms: sporadic (sALS) and familial (fALS), the latter accounting for 5-10% of the whole ALS population, and at least fifteen genes involved in different cellular pathways have been related to ALS [7]. About 25% of the total fALS cases are due to mutations in the gene encoding Cu/Zn superoxide dismutase type 1 (SOD1). More than 100 distinct SOD1 mutations have been identified [8], the most abundant of which is the substitution of glycine in position 93 with alanine (G93A).Accordingly, the $SOD1^{G93A}$ mutation-expressing mouse represents at present the most popular animal model to study human ALS [9].

Different cellular and molecular mechanisms have been proposed to concur to motor neuron death in ALS, including glutamate induced excitotoxicity, endoplasmic reticulum stress, proteasome inhibition, secretion of detrimental factors by non-neuronal cells, oxidative stress, axonal disorganization, neuromuscular junction abnormalities, aberrant RNA processing, and mitochondria-mediated damage [10–18].

As to the last item, several authors reported alterations of energy metabolism in ALS animal models, as well as in ALS patients [19, 20]. Electron transport chain (ETC) defects were observed [21–27], determining an impairment of mitochondrial energy metabolism, also before the clinical onset of the pathology [20]. Furthermore, mitochondria show altered morphology in skeletal muscle,

liver, spinal cord and motor cortex neurons [28–30] as well as a defect in Ca^{2+} buffering [21, 23]. Modifications of the metabolic equilibrium has been also demonstrated in NSC34 cells expressing the *SOD1*^{G37R} or the *SOD1*^{G93A}mutation [29, 31]. All the above findings support the assumption that alteration of energy metabolism could play a pivotal role in ALS onset and progression, but, at present, the synergic contribution of neurons and glia has not been fully characterized.

Strong evidence from literature highlights the role of astrocytes, microglia and oligodendrocytes in ALS, supporting the idea that this is a non-cell autonomous disease [32, 33]. In particular, astrocytes, surrounding the pre- and postsynaptic elements, are considered a key component of the synapse domain, playing an essential role in regulating the synaptic function, strength and plasticity [34–36]. Interestingly, the interaction between astrocytes and the neighbouring motor neurons, in terms of trophic support and metabolic activity, may be altered in ALS [37, 38]. In this scenario, it has been demonstrated that *SOD1*^{G93A} mouse-derived astrocytes can induce defects in mitochondria of motor neurons and reduce neuronal survival [38–40].

We previously reported that glutamate release elicited from nerve terminals by exocytotic and non-exocytotic mechanisms is abnormal in *SOD1*^{G93A}mouse spinal cord [41–44]. This excessive release of glutamate occurs as early as in 30 days-old mice [42, 45] and is supported by profound modifications of the presynaptic release machinery [44–46]. Interestingly, the abnormal glutamate release was observed also in *SOD1*^{G93A} mouse spinal cord astrocyte preparations and it was very precocious during the disease development [47].

Along this view, we have focused our attention on the mitochondrial metabolism of the pre-synapse and of the astroglial districts deputed to the neuro- and glio-transmission; i.e. those astrocytic regions surrounding the synapse itself (perisynaptic astrocyte processes; PAP). In particular, we have exploited the characteristics of synaptosomes, as an in-vitro model of presynaptic axon terminals [48, 49] and of gliosomes, as an in-vitro model of PAP, that has been fully characterized by our research group [50–52]. The data obtained show that bioenergetics is impaired in spinal cord axon terminals of *SOD1*^{G93A} mice, already before the clinical onset of the pathology, while PAP of *SOD1*^{G93A} mice

display a little decrement of the ATP/AMP ratio at the late phase of the disease, only. These results support the idea that these two districts may differently contribute to the synaptic damage in ALS.

MATERIALS AND METHODS

Reagents

All chemicals were purchased from Sigma Aldrich (St. Louis, MO, USA), unless otherwise indicated. Ultrapure water (Milli-Q; Millipore, Billerica, MA, USA) was used throughout. All other reagents were of analytical grade.

Animals

B6SJL-TgN SOD1/G93A(+)1Gur mice expressing high copy number of mutant human SOD1 with a $Gly^{93}Ala$ substitution [$SOD1^{G93A}$] and B6SJL-TgN (SOD1)2Gur mice expressing wild-type human SOD1 (*wtSOD1*)[53] were originally obtained from Jackson Laboratories (Bar Harbor, ME) and bred at the animal facility of the Pharmacology and Toxicology Unit, Department of Pharmacy in Genoa. Transgenic animals have been crossed with background-matched B6SJL wild type female and selective breeding maintained each transgene in the hemizygous state. All transgenic mice were identified analyzing tissue extracts from tail tips as previously described[54]. Tissue was homogenized in phosphate-buffer saline, freeze/thawed twice and centrifuged at 23,000 x *g* for 15 min at 4° C and the human SOD1 was evaluated by staining for its enzymatic activity after 10% non-denaturing polyacrylamide gel electrophoresis. Animals were housed at constant temperature (22 ± 1°C) and relative humidity (50%) with a regular 12 h-12 h light cycle (light 7 AM-7 PM), throughout the experiments. Food (type 4RF21 standard diet obtained from Mucedola, Settimo Milanese, Milan, Italy) and water were freely available. Sexes were balanced in each experimental group to avoid bias due to sex-related intrinsic differences. For experimental use, animals were sacrificed at different

stages of disease, according to their age. Experiments were carried out in accordance with the guidelines established by the European Communities Council (EU Directive 114 2010/63/EU for animal experiments published on September 22nd, 2010) and with the Italian D.L. n. 26/2014, and were approved by the local Ethical Committee and by the Italian Ministry of Health (Project Authorization No. 31754-3-2013 and project No. 75f11.2, Authorization No.97/2017-PR). All efforts were made to minimize animal suffering and to use only the number of animals necessary to produce reliable results. All the performed experiments using animals comply with the ARRIVE guidelines. A total number of 27*wtSOD1* and 30 $SOD1^{G93A}$, mice were utilized in this study.

Purification of synaptosomes and gliosomes

*wtSOD1*and $SOD1^{G93A}$mice (30, 60, 90, and 120 days old) were euthanized and the different central nervous system tissues (motor cortex, hippocampus, cerebellum and spinal cord) rapidly removed. Synaptosomes and gliosomes were prepared essentially as previously described [51]. The tissue was homogenized in 0.32 M sucrose, buffered at pH 7.4 with Tris-HCl, using a glass-teflon tissue grinder (clearance 0.25 mm - Potter-Elvehjem VWR International). The homogenate was centrifuged (5 min, 1,000 x *g*) to remove nuclei and debris. The supernatant was harvested and centrifuged at 12,000 x *g* for 10 min and the pellet was resuspended in Tris-buffered0.32 M sucrose and gently layered on a discontinuous Percoll® (Sigma-Aldrich, St Louis, Missouri, USA) gradient (2, 6, 10 and 20% v/v in Tris-buffered 0.32 M sucrose). After centrifugation at 33,500 x *g* for 5 min, the layer between 2 and 6% (gliosomal fraction) and between 10 and 20% (synaptosomal fraction) Percoll® were collected and washed by centrifugation at 20,000xg for 15 min with phosphate buffer saline (PBS). Gliosomal and synaptosomal pellets were resuspended in PBS in the presence of 20mM glucose for bioenergetics determinations or in lysis buffer for western blotting. All the above procedures were conducted at 4°C. Protein content was measured according to Bradford [55], using bovine serum albumin (Sigma-Aldrich, St Louis, Missouri, USA) as a standard.

Assay of intracellular ATP and AMP levels

Quantification of ATP and AMP was based on the enzyme coupling method. 20 µg of total protein of mouse synaptosomes or gliosomes from 30, 60, 90, and 120 days-old *wtSOD1* and *SOD1*^{G93A} mice were used. Briefly, ATP was assayed spectrophotometrically at 340 nm, following NADP reduction. Medium contained 50 mM Tris-HCl pH 8.0, 1 mM NADP, 10 mM $MgCl_2$, and 5 mM glucose in 1 ml final volume. Samples were analysed before and after the addition of 4 µg of purified hexokinase plus glucose-6-phosphate dehydrogenase. AMP was assayed spectrophotometrically at 340 nm, following NADH oxidation. Medium contained 100 mM Tris-HCl pH 8.0, 75 mM KCl, 5 mM $MgCl_2$, 0.2 mM ATP, 0.5 mM phosphoenolpyruvate, 0.2 mM NADH, 10 IU adenylate kinase, 25 IU pyruvate kinase, and 15 IU of lactate dehydrogenase [56].

Oxymetric analysis

Oxygen consumption was measured with an amperometric oxygen electrode in a closed chamber, magnetically stirred at 37 °C. For each assay, 50 µg of total protein of mouse spinal cord synaptosomes and gliosomes from 30, 60, 90, and 120 days old *wtSOD1* and *SOD1*^{G93A}mice were used. After permeabilization with 0.03 mg/ml digitonin for 10 minutes, sampleswere suspended in a medium containing 137 mM NaCl, 5 mM KH_2PO_4, 5 mM KCl, 0.5 mM EDTA, 3 mM $MgCl_2$ and 25 mM Tris–HCl, pH 7.4. To activate the pathway composed by Complexes I, III and IV, 5 mM pyruvate + 2.5 mM malate were added. To activate the pathway composed by Complexes II, III and IV, 20 mM succinate was used [57].

Respiratory complexes activity assay

The activity of the redox complexes I, II, III and IV was measured on 50 µg of mouse spinal cord synaptosomes and gliosomes from 30, 60, 90, and 120 days old *wtSOD1* and *SOD1*^{G93A}mice.

Complex I (NADH-ubiquinone oxidoreductase) was assayed following the reduction of ferricyanide at 420 nm; the reaction mixture was composed by: 10 mM phosphate buffer pH 7.2, 30 mM NADH, 40 mM ferricyanide, 40 μM antimycin A.

Complex II (Succinic dehydrogenase) activity was measured at 600 nm, in 2 mM EDTA, 0.2 mM ATP, 20 mM succinate, 0.5 mM cyanide, 80 μM dicloroindophenol (DCIP), 50 μM decylubiquinone, 40 μM antimycin A, 10 μM rotenone and 10 mM phosphate buffer, pH 7.2. Complex III (Cytochrome c reductase) activity was measured at 550 nm followed the reduction of oxidized Cytochrome c. The reaction mixture containing: 10 mM phosphate buffer pH 7.2, 0.03% oxidized cytochrome C and 0.5 mM KCN. Complex IV (Cytochrome c oxidase) was assayed following the oxidation of ascorbate-reduced Cytochrome c at 550 nm, in a solution containing 10 mM phosphate buffer pH 7.2, 0.03/ reduced cytochrome C and 40 μM antimycin A

Evaluation F_1F_o-ATP synthase activity

F_1F_o-ATP synthase activity was detected by measuring ATP production by the highly sensitive luciferin/luciferase method. Assays was conducted at 37°C, over 2 min, by measuring ATP produced from di-adenosine-5'penta-phosphate (ADP). 50 μg of total protein of mouse spinal cord synaptosomes and gliosomes from 30, 60, 90, and 120 days-old *wtSOD1*and *SOD1*^{G93A}mice were added to the incubation medium (0.1 ml final volume), which contained 10 mM Tris-HCl pH 7.4, 50 mM KCl, 1 mM EGTA, 2 mM EDTA, 5 mM KH_2PO_4, 2 mM $MgCl_2$, 0.6 mM ouabain, 0.040 mg/ml ampicillin, 0.2 mM ADP and the metabolic substrates (5 mM pyruvate + 2.5 mM malate or 20 mM succinate). Cells were equilibrated for 10 min at 37°C, then ATP synthesis was induced by addition of 0.2 mM ADP. ATP synthesis was measured using the luciferin/luciferase ATP bioluminescence assay kit CLSII (Roche, Basel, Switzerland), on a Luminometer (GloMax® 20/20 Luminometer – Promega, Wisconsin, USA). ATP standard solutions (Roche, Basel, Switzerland) in the concentration range 10^{-10} - 10^{-7} M were used for calibration [58].

Malondialdehyde assay

To assess the extent of lipid peroxidation, the levels of malondialdehyde (MDA) were evaluated using the thiobarbituric acid reactive substances (TBARS). The TBARS solution contained: 15% trichloroacetic acid in 0.25 N HCl and 26 mM 2-Thiobarbituric acid. To evaluate the basal concentration of MDA, 600 µl of TBARS solution were added to 50 µg of total protein of mouse spinal cord synaptosomes and gliosomes from 30, 60, 90, and 120 days old *wtSOD1* and *SOD1*^{G93A} mice dissolved in 300 µl of water. Synaptosomes and gliosomes were incubated for 40 min at 100°C, then centrifuged at 20,000 x *g* for 2 min and the supernatant analysed spectrophotometrically at 532 nm [59].

Western Blotting

Mouse spinal cord synaptosomes and gliosomes from 30, 60, 90, and 120 days-old *wtSOD1* and mice *SOD1*^{G93A}mice were lysed and used for Western blot analyses. Protein extracts (20 µg) were loaded onto 8-20% gradient polyacrylamide gel (BioRad, Hercules, California, USA), separated by SDS-PAGE, and transferred to nitrocellulose membranes. Non-specific membrane binding sites were saturated in 5% skimmed-milk solution and membranes were incubated over-night at 4 °C with the following primary antibodies: rabbit anti-ATP5B 1:500 (a subunit of F_1 moiety of ATP synthase, Sigma Aldrich, Saint Louis, Missouri, USA), antiMT-CO2 (a subunit of respiratory complex IV, Abcam, Cambridge, UK), anti-mitochondrial import inner membrane translocase, subunit8A (TIM, Santa Cruz Biotechnology, California, USA) and mouse anti-Gapdh 1:5000 (Sigma Aldrich, Saint Louis, Missouri, USA). After washing, membranes were incubated for 60 min at room temperature with the following peroxidase-coupled secondary antibodies: goat anti-rabbit 1:2000 (Sigma Aldrich, Saint Luis, Missouri, USA). Bands were detected and analyzed for optical density using an enhanced chemiluminescence substrate (ECL, LiteAblot PLUS, Euroclone, Milan, Italy) and a

chemiluminescence system (Alliance 6.7 WL 20M, UVITEC, Cambridge, UK), and UV1D software (UVITEC). Bands of interest were normalized for Gapdh level in the same membrane.

Electron microscopy

For ultrastructural analysis, synaptosomes were fixed in 2.5% glutaraldehyde in cacodylate buffer 0.1 M, pH 7.2, postfixed in 1% osmium tetroxide in cacodylate buffer 0.1 M, pH 7.2, en bloc stained with a 1% aqueous solution of uranyl acetate, dehydrated through a graded ethanol series. Samples were then embedded in LX112 (Polysciences Inc., Warrington, PA, USA), polymerized for 12 h at 42 °C, followed by 48 h at 60 °C. Gray–silver ultrathin sections, obtained using a Leica Ultracut E microtome, were stained with uranyl acetate and lead citrate, and analyzed with a FEI CM10 electron microscopy. To quantify the number of mitochondria, 12 electron micrographs were obtained at 8,900× from ultrathin sections of each sample [43]. Seventy synaptosomes and contained mitochondria were examined for each sample. To evaluate the ratio of mitochondria surface and total synaptosomes surface, Image J software (U. S. National Institutes of Health, Bethesda, Maryland) has been employed.

Statistics

Data are expressed as mean ± s.e.m. and p value < 0.05 was considered significant. Statistical comparison of two means were performed by unpaired two-tailed Student's t-test while multiple comparisons were performed using the analysis of variance (two-way ANOVA) followed by Bonferroni post hoc test. Analyses were performed by means of SigmaStat (Systat Software, Inc., San Jose, CA, USA) software.

RESULTS

ATP/AMP ratio in synaptosomes and gliosomes from SOD1^{G93A} mouse spinal cord, motor cortex, hippocampus and cerebellum.

Figure 1 shows the ATP/AMP ratio, a marker of the chemical energy status, in synaptosomes and gliosomes (Panels A and B, respectively) isolated from spinal cord of *SOD1^{G93A}* and *wtSOD1* control mice. Synaptosomes from spinal cord of *SOD1^{G93A}*mice displayed a significant reduction in ATP/AMP ratio in comparison to *wtSOD1* control mice ($p<0.001$, $F_{(3,1,3,16)}=0.777$ at 30, 60, 90 and 120 days of age). By contrast, such reduction was less evident in gliosomes, being significantly detectable in *SOD1^{G93A}*mice only at day 90 ($p<0.05$, $F_{(3,1,3,16)}=2.039$) and 120 ($p<0.05$, $F_{(3,1,3,16)}=2.039$). Of note, the ATP/AMP ratio was unmodified in synaptosomes isolated from the motor cortex, hippocampus and cerebellum of 90 days old *SOD1^{G93A}* mice, with respect to control mice (Fig. 1C); the same was true also in gliosomes purified from the above brain regions (Fig. 1D).

Thus, the chemical energy supply appears strongly and precociously reduced in the nerve terminal and, less so, in the perisynaptic astrocyte compartment. Moreover, the energy impairment of the presynaptic district is apparently restricted to spinal cord, suggesting that the alterations of mitochondrial metabolism observed in the brain of *SOD1^{G93A}*mice [21, 60] may be ascribed to other parts of neurons.

Oxygen consumption and activity of the respiratory complexes in synaptosomes and gliosomes from SOD1^{G93A} mouse spinal cord.

Since mitochondria are the principal source of ATP, through the OxPhos metabolism, the oxygen consumption was evaluated in synaptosomes and gliosomes from the spinal cord of *SOD1^{G93A}* and *wtSOD1* mice at 30, 60, 90 and 120 days of life.

Oxygen consumption induced with pyruvate+malate was significantly reduced in *SOD1^{G93A}* synaptosomes at any time point analysed ($p<0.001$, $F_{(3,1,3,16)}=8.859$ at 30, 60, 90 and 120 days) (Fig.2A). Actually, a significant reduction of the pyruvate+malate-induced oxygen consumption could be observed also in *wtSOD1* mice at day 120 when compared to day 30 ($p<0.001$, $F_{(3,\ 1,\ 3,}$

$_{16)}$=8.859). The same significant reduction of oxygen consumption was detected in *SOD1^{G93A}* mouse synaptosomes in the presence of succinate ($p<0.001$, $F_{(3,1,3,16)}=2.93$ at 30, 60, 90 and 120 days) (Fig. 2C), but not in gliosomes (Fig. 2D). The succinate induced oxygen consumption was diminished also in *wtSOD1* mice at day 90 and 120 ($p<0.01$ $F_{(3,1,3,16)}=2.93$*vs.* day 30) (Fig 2C). Conversely, no changes were detected in gliosomes in the presence of pyruvate+malate (Fig 2B) or of succinate (Fig. 2D).

To evaluate whether the alterations of OxPhos depend on a specific respiratory complex or on the entire ETC, the activities of the four respiratory complexes were analysed in 30, 60, 90, and 120 days-old *SOD1^{G93A}* and *wtSOD*1 mice.

Figure 3A shows that the activity of Complex I was compromised in *SOD1^{G93A}* mice at all stages of the pathology ($p<0.001$, $F_{(3,1,3,16)}=13.049$ at 30, 60, 90 and 120 days). Similar reduction patterns were displayed also by Complex II ($p<0.001$, $F_{(3,1,3,16)}=10.802$ at 30, 60 and 90 days; $p<0.05$, $F_{(3,1,3,16)}=10.802$ at 120 days) (Fig. 3C), Complex III ($p<0.001$, $F_{(3,1,3,16)}=18.16$ at 30, 60, 90 and 120 days) (Fig. 3E) and Complex IV $p<0.001$, $F_{(3,1,3,16)}=17.214$ at 30, 60, 90 and 120 days) (Fig. 3G) in synaptosomes from *SOD1^{G93A}* respect to *wtSOD1* mice. Reduction of the respiratory complex activities were observed in *wtSOD1* mice at day 120 vs. day 30 as to Complex I ($p<0.001$ $F_{(3,1,3,16)}=13.049$) and Complex II ($p<0.001$, $F_{(3,1,3,16)}=10.802$) (Fig. 3A and Fig. 3C) and at day 90 and 120 *vs*. day 30 as to Complex III ($p<0.001$, $F_{(3,1,3,16)}=18.16$ at 90 and 120 days) (Fig. 3 E) and Complex IV ($p<0.001$, $F_{(3,1,3,16)}=17.214$ at 90 and 120 days) (Fig. 3G). Conversely, no differences could be observed in gliosomes from *SOD1^{G93A}* and *wtSOD1* mice in the case of Complex I (Fig. 3B), Complex II (Fig. 3D), Complex III (Fig. 3F) and Complex IV (Fig. 3H).

Thus, as for ATP/AMP ratio, the oxygen consumption and the activity of the four respiratory Complexes are impaired in *SOD1^{G93A}* spinal cord synaptosomes but not in gliosomes.

F_1F_o-ATP synthase activity in synaptosomes and gliosomes from SOD1^{G93A} mouse spinal cord.

Oxygen consumption is associated to the proton gradient formation, necessary to synthetize ATP trough F_1F_o-ATP synthase [61]. Therefore, to evaluate if the impairment of ETC activity,

observed in *SOD1^{G93A}* mouse synaptosomes, causes a decrement in the ATP production, we measured the synthesis of ATP induced by pyruvate+malate or by succinate, as an index of the F_1F_o-ATP synthase activity.

ATP synthesis was significantly reduced in spinal cord *SOD1^{G93A}* mouse synaptosomes, both in the presence of pyruvate+malate ($p<0.001$, $F_{(3,1,3,16)}=2.222$ at 30 and 60 days; $p<0.01$, $F_{(3,1,3,16)}=2.222$ at 90 and 120) (Fig. 4A) or succinate ($p<0.001$, $F_{(3,1,3,16)}=5.989$ at 30, 60, 90 and 120 days) (Fig. 4C). As shown above for oxygen consumption, also ATP synthesis induced by pyruvate+malate in *wtSOD1* mice was diminished at day 120 ($p<0.001$, $F_{(3,1,3,16)}=5.989$ *vs.* day 30) (Fig 4A) and that induced by succinate at day 90 and 120 ($p<0.001$, $F_{(3,1,3,16)}=5.989$*vs.* day 30) vs. day 30 (Fig 4C). Once again, *SOD1^{G93A}* mouse gliosomes did not show changes, when ATP synthesis was induced by pyruvate+malate (Fig. 4B) or by succinate (Fig. 4D).

Thus, F_1F_o-ATP synthase activity is reduced in of *SOD1^{G93A}* spinal cord synaptosomes but not in gliosomes, supporting the data shown in the previous experiments, although ATP synthase expression barely couples with the ATP supply reduction.

Mitochondrial presence and TIM, MT-CO2 and β subunit of ATP synthase expression in synaptosomes from SOD1^{G93A} mouse spinal cord.

ALS animal models show altered mitochondrial localization in synapses and Ranvier nodes due to defects in the axonal transport [62, 63]. In order to determine whether the decrement of OxPhos activity in synaptosomes of *SOD1^{G93A}* mice could be caused by a reduced presence of mitochondria at the terminal level, we analysed the number and the area occupied by mitochondria in spinal cord synaptosomes from *SOD1^{G93A} and wtSOD1* mice at 120 days of life. Data show that both the number of mitochondria (Fig. 5B) and the mitochondrial area (Fig. 5C) did not differ significantly in *SOD1^{G93A} and wtSOD1* mice. The same results have been obtained measuring the expression of TIM, a typical inner mitochondrial membrane protein not involved in the aerobic metabolism [64]: TIM

expression was similar in *SOD1*^{G93A} mice synaptosomes with respect to control samples (Figure 5D and 5E).

It should be noted, however, that the most part (around 60%) of mitochondria in synaptosomes purified from *SOD1*^{G93A} mice appeared swollen, with cristae less defined, in comparison with those observed in control synaptosomes (Fig. 5A for representative images).

Therefore, to evaluate if the altered OxPhos observed in synaptosomes from *SOD1*^{G93A} mice may depend by a lower content of the proteins involved in the aerobic metabolism, the expression of MT-CO2 (Figure 5D and 5F), a subunit of complex IV [65], and β subunit of ATP synthase (Figure 5D and 5G) has been analysed. No differences were observed in the expression of the two proteins in *SOD1*^{G93A} mouse synaptosomes when compared to *wtSOD1* control mice.

Thus, these data support the idea that the reduced aerobic metabolism in synaptosomes of *SOD1*^{G93A} mice does not derive from a reduced number of mitochondria or from altered expression of OxPhos proteins, but could depend by an alteration of mitochondrial morphology.

Lipid peroxidation in synaptosomes and gliosomes from SOD1^{G93A} *mouse spinal cord.*

Finally, considering that dysfunctions of mitochondrial aerobic metabolism are associated with massive oxidative stress production [66], we evaluated the MDA levels as a marker of lipid peroxidation in synaptosomes and gliosomes isolated from spinal cord of 30, 60, 90, and 120 days-old *SOD1*^{G93A} and *wtSOD1* mice.

MDA content was higher than in controls in both *SOD1*^{G93A} mouse synaptosomes ($p<0.01$, $F_{(3,1,3,16)}=0.259$ at 30, 90 and 120 days; $p<0.001$, $F_{(3,1,3,16)}=0.259$ at 60 days) (Fig. 6A) and gliosomes ($p<0.01$, $F_{(3,1,3,16)}=1.509$ at 30, 60 and 90 days: $p<0.001$, $F_{(3,1,3,16)}=1.509$ at 120 days) (Fig. 6B). MDA concentration increased with animal age also in synaptosomes from *wtSOD1* mice, being significant at day 120 ($p<0.01$, $F_{(3,1,3,16)}=0.259$ *vs*. day 30). The same tendency was observed in gliosomes, even though the increase was quantitatively lower compared to the neuronal counterpart.

Thus, the high MDA content in synaptosomes from *SOD1*^{G93A} mice suggests that the dysfunction of aerobic metabolism is associated with an increment in lipid peroxidation, a sign of enhanced ROS production. Also gliosomes from *SOD1*^{G93A} mice show an increment of MDA level, although this event does not seem linked to the alteration of OxPhos function.

DISCUSSION

In the present work, for the first time, we characterised the alteration of mitochondrial energy metabolism in synaptic nerve terminals and perisynaptic astroglial processes isolated from the spinal cord of *SOD1*^{G93A} mice, at different stages of the disease. We focused our attention on those districts because, in face of the already reported ALS-associated energy impairment [15, 29, 67], less is known about the distinct contribution of neurons and glia, in particular at the synaptic level. Data show specific presynaptic energy metabolism dysfunctions, due to OxPhos impairment and oxidative stress production.

To study the pre- and perisynaptic energy metabolism we exploited the characteristics of two acutely-purified ex-vivo preparations, i.e. synaptosomes and gliosomes. Synaptosomes, that are the site of neurotransmitter release, are pinched-off nerve terminals acutely prepared here from the spinal cord and other brain regions of differently aged *wtSOD1* and *SOD1*^{G93A} mice. It has been widely demonstrated that isolated synaptosomes retain most of the characteristics of the nerve terminals *in-vivo*. They express functional ionic channels to provide the correct neuronal membrane potential, which undergoes depolarization upon chemical stimulation, possess the machinery to synthetize and release neurotransmitters, store functional mitochondria, express release-regulating receptors and transporters to sense or recapture the released neurotransmitters, respectively [48, 49, 68]. It is also well known that astrocytes play a pivotal role in affecting motor neuron wellness and viability in ALS [32, 69]. To investigate this important issue, we took advantage of gliosomes, a subcellular preparation of astrocytic origin, purified during synaptosome isolation [51]. We and others have

demonstrated that the gliosomal preparation expresses astrocytic but not neuronal, microglial or oligodendroglial markers [51, 52]. In addition, gliosomes possess a large amount of the biochemical and functional characteristics of astrocytes *in-situ*: they contain proteins and vesicles for exocytosis, operate gliotrasmitter uptake and release [50, 51, 70] and, likely, represent the astrocytic regions surrounding the synapses, since a recent proteomic study revealed that they are enriched in proteins distinctive of the PAP [52]. Therefore, purified synaptosomes and gliosomes represent a unique tool to investigate the bioenergetic signature of the presynaptic and perisynaptic compartments of the tripartite synapse and to reveal changes across the ALS disease course.

Data reported herein show that the energetic metabolism was impaired in $SOD1^{G93A}$-derived spinal cord synaptosomes, but not in $SOD1^{G93A}$ mouse cortex, hippocampus or cerebellum synaptosomes, suggesting that this presynaptic phenomenon specifically occurs in the spinal cord. Interestingly, the deficit of OxPhos activity in spinal cord synaptosomes was already evident at the very early stage of the disease (30 days-old $SOD1^{G93A}$ mice), well before the onset of clinical symptoms, and span along the whole animal life, supporting the view that it may represent a cause of the presynaptic pathological changes rather than a consequence of the disease progression. Even though the intracellular ATP concentration depends on different biochemical pathways, the principal source of ATP is the aerobic metabolism, occurring in mitochondria; thus, to shed light on the energetic impairment of the neuronal presynaptic district, we evaluated the mitochondrial function in synaptosomes isolated from $SOD1^{G93A}$ mice. We observed a decrement of oxygen consumption, both in the presence of pyruvate+malate or succinate, already in the 30 days-old mice, suggesting that the entire ETC was not performing appropriately. This assumption was confirmed by assays of the activities of the four respiratory complexes, which appeared to be impaired in a very similar way at any age during disease progression. These metabolic alterations did not depend on different expression of the OxPhos proteins, as shown by the WB analyses assessing the expression of the β subunit of F_1Fo-ATP synthase [61] and MT-CO2 [65]. Moreover, also the synaptosomal mitochondrial content was similar in $SOD1^{G93A}$ synaptosomes with respect to the control samples, as

suggested by the expression levels of TIM, a typical mitochondrial inner membrane protein not involved in the aerobic metabolism [64] and by the stereological analyses.

It is well known that OxPhos activity is related to the integrity of the mitochondrial membrane [71, 72]; any alteration of this lipid-based structure, as occurs in the case of high lipid peroxidation, may impair ATP synthesis. This occurrence can increment, in turn, the oxidative stress production [66, 73, 74], being the ETC a major ROS producer [75, 76]. Along this line, we observed that the morphology of mitochondria of *SOD1*^{G93A} mouse synaptosomes appeared altered with respect to the control and that the MDA content was increased in *SOD1*^{G93A} mouse synaptosomes compared to *wtSOD1*mice.

Summarizing, in our experiments, the altered ETC activity has two consequences on cellular metabolism of *SOD1*^{G93A} mice: first, it determines a reduction of F_1F_o-ATP synthase activity, thus reducing the ATP production and favouring a decrease of the ATP/AMP ratio; second, it increases oxidative stress. These events determine a vicious circle, which increments the OxPhos dysfunction, causing endoplasmic reticulum stress, proteasome inhibition and ultimately axonal disorganization [66, 77]. Accordingly, it has been reported that mutant SOD1 induces ROS and nitric oxide production in mitochondria and promotes cytochrome C release, activating caspase-dependent cell death mechanisms [23].

The metabolic alterations observed in synaptosomes were not replicated in gliosomes. In particular, gliosomes did not show a substantial decrement of the OxPhos activity, except for the impairment of ATP/AMP ratio at the symptomatic stage of the disease, in 90 and 120 days-old *SOD1*^{G93A}mice. However, lipid peroxidation appeared higher in gliosomes from *SOD1*^{G93A}mice , already at 30 days of age, although this occurrence does not seem linked to the alteration of OxPhos function. The lack of metabolic alterations in the presymptomatic phase of the disease suggests that *SOD1*^{G93A} mouse-derived astrocytic gliosomes do not suffer metabolic impairment, at least at the early phases of the disease.

The differences observed between synaptosomes and gliosomes leads us to hypothesize that the energy metabolism alterations in the perisynaptic compartment of the tripartite synapse may be subordinated to neuronal damage, which would play a primary role although the importance of astrocyte for motor neuron injury in ALS has been widely reported and different mechanisms have been investigated [39, 78, 79]. As to the energetic metabolism here studied, perisynaptic astrocytes seem to be bystanders, contributing to synapse impairment as a consequence of a deleterious cycle starting in nerve terminals. Whether this consequentiality is not restricted to the presynaptic and perisynaptic structures but represents also a characteristic of motor neuron and astrocyte cells is worth investigating.

Correlations between the impairment of the OxPhos in synaptosomes, here described, and the previously reported abnormal glutamate exocytosis in *SOD1*^{G93A} mice (see [45] and references therein) are not obvious. Considering that glutamate release is a highly energy-dependent mechanism, it is possible to speculate that the impairment of ATP production in *SOD1*^{G93A} mice, paralleled by the increment of the activity of the glutamate release machinery, determines a stress condition, which could favour synaptic damage and neuron degeneration. These events likely occur all over the central nervous system during the disease progression; however, it is widely established that MNs are particularly prone to energetic metabolism failure, because of their huge need of energy supply due to their unique morphology and to the particular sensitivity to the increase of calcium levels, due to impaired Ca^{2+} buffering processes. Our results imply that upper motor neuron nerve terminals in the spinal cord, differently from PAP, are strongly and precociously affected by excessive neurotransmitter release activity and concomitant energy impairment.

In conclusion, the present results suggest that nerve endings are a primary site of defective energy metabolism within the spinal cord and point to the synaptic energy metabolism as a key aspect to explore, in light of potential neuroprotective strategies, effective also in hindering the propagation of bioenergetics impairment from MNs to astrocytes.

Acknowledgements

The Authors are indebted to Mr. Giuseppe Marazzotta for his help in maintaining the *SOD1*^{G93A}and the *wtSOD1* mouse colonies.The authors gratefully acknowledge the undergraduate students Cesare Cecchini, Mirna Nitro and Roncallo Roberta, for their helpful technical support.

Funding

This work was supported by research grants from the Italian Ministry of University (PRIN project n. 2016058401 to GB, and SIR project n. RBSI14B1Z to M.M.) and from Motor Neuron Disease Association (project n. April16/848-791) to GB.

Conflict of interest

The authors declare no competing financial interests.

REFERENCES

1. Brown Jr. RH (1995) Superoxide dismutase in familial amyotrophic lateral sclerosis: models for gain of function. Curr Opin Neurobiol 5:841–846. doi: 0959-4388(95)80114-6 [pii]
2. Eisen A (2009) Amyotrophic lateral sclerosis-Evolutionary and other perspectives. Muscle Nerve 40:297–304. doi: 10.1002/mus.21404
3. Rowland LP, Shneider NA (2001) Amyotrophic Lateral Sclerosis. N Engl J Med 344:1688–1700. doi: 10.1056/NEJM200105313442207
4. Turner MR, Bowser R, Bruijn L, et al. (2013) Mechanisms, models and biomarkers in amyotrophic lateral sclerosis. Amyotroph Lateral Scler Front Degener 14:19–32. doi: 10.3109/21678421.2013.778554
5. Lu H, Le WD, Xie Y-Y, Wang X-P (2016) Current Therapy of Drugs in Amyotrophic Lateral Sclerosis. Curr Neuropharmacol 14:314–21.
6. Abe K, Aoki M, Tsuji S, et al. (2017) Safety and efficacy of edaravone in well defined patients with amyotrophic lateral sclerosis: a randomised, double-blind, placebo-controlled trial. Lancet Neurol 16:505–512. doi: 10.1016/S1474-4422(17)30115-1
7. Andersen PM, Al-Chalabi A (2011) Clinical genetics of amyotrophic lateral sclerosis: what do we really know? Nat Rev Neurol 7:603–615. doi: 10.1038/nrneurol.2011.150
8. Kaur SJ, McKeown SR, Rashid S (2016) Mutant SOD1 mediated pathogenesis of Amyotrophic Lateral Sclerosis. Gene 577:109–18. doi: 10.1016/j.gene.2015.11.049
9. Philips T, Rothstein JD (2015) Rodent Models of Amyotrophic Lateral Sclerosis. Curr Protoc Pharmacol 69:5.67.1-21. doi: 10.1002/0471141755.ph0567s69
10. Cleveland DW, Bruijn LI, Wong PC, et al. (1996) Mechanisms of selective motor neuron death in transgenic mouse models of motor neuron disease. Neurology 47:S54-61–2.
11. Morrison BM, Morrison JH (1999) Amyotrophic lateral sclerosis associated with mutations

in superoxide dismutase: a putative mechanism of degeneration. Brain Res Brain Res Rev 29:121–35.

12. Van Den Bosch L, Van Damme P, Bogaert E, Robberecht W (2006) The role of excitotoxicity in the pathogenesis of amyotrophic lateral sclerosis. Biochim Biophys Acta - Mol Basis Dis 1762:1068–1082. doi: 10.1016/j.bbadis.2006.05.002

13. Matus S, Valenzuela V, Medinas DB, Hetz C (2013) ER Dysfunction and Protein Folding Stress in ALS. Int J Cell Biol 2013:1–12. doi: 10.1155/2013/674751

14. Droppelmann CA, Campos-Melo D, Ishtiaq M, et al. (2014) RNA metabolism in ALS: When normal processes become pathological. Amyotroph Lateral Scler Front Degener 15:321–336. doi: 10.3109/21678421.2014.881377

15. Tan W, Pasinelli P, Trotti D (2014) Role of mitochondria in mutant SOD1 linked amyotrophic lateral sclerosis. Biochim Biophys Acta - Mol Basis Dis 1842:1295–1301. doi: 10.1016/j.bbadis.2014.02.009

16. Peters OM, Ghasemi M, Brown RH (2015) Emerging mechanisms of molecular pathology in ALS. J Clin Invest 125:1767–1779. doi: 10.1172/JCI71601

17. King AE, Woodhouse A, Kirkcaldie MTK, Vickers JC (2016) Excitotoxicity in ALS: Overstimulation, or overreaction? Exp Neurol 275:162–171. doi: 10.1016/j.expneurol.2015.09.019

18. CarrÃ¬ MT, Valle C, Bozzo F, Cozzolino M (2015) Oxidative stress and mitochondrial damage: importance in non-SOD1 ALS. Front Cell Neurosci 9:41. doi: 10.3389/fncel.2015.00041

19. Dupuis L, Pradat PF, Ludolph AC, Loeffler JP (2011) Energy metabolism in amyotrophic lateral sclerosis. Lancet Neurol 10:75–82. doi: 10.1016/S1474-4422(10)70224-6

20. Browne SE, Yang L, DiMauro JP, et al. (2006) Bioenergetic abnormalities in discrete cerebral motor pathways presage spinal cord pathology in the G93A SOD1 mouse model of ALS. Neurobiol Dis 22:599–610. doi: 10.1016/j.nbd.2006.01.001

21. Mattiazzi M, D'Aurelio M, Gajewski CD, et al. (2002) Mutated human SOD1 causes dysfunction of oxidative phosphorylation in mitochondria of transgenic mice. J Biol Chem 277:29626–33. doi: 10.1074/jbc.M203065200

22. Ferri A, Cozzolino M, Crosio C, et al. (2006) Familial ALS-superoxide dismutases associate with mitochondria and shift their redox potentials. Proc Natl Acad Sci U S A 103:13860–5. doi: 10.1073/pnas.0605814103

23. Kawamata H, Manfredi G (2010) Mitochondrial dysfunction and intracellular calcium dysregulation in ALS. Mech Ageing Dev 131:517–526. doi: 10.1016/j.mad.2010.05.003

24. Ferri A, Nencini M, Cozzolino M, et al. (2008) Inflammatory cytokines increase mitochondrial damage in motoneuronal cells expressing mutant SOD1. Neurobiol Dis 32:454–60. doi: 10.1016/j.nbd.2008.08.004

25. Cozzolino M, Pesaresi MG, Amori I, et al. (2009) Oligomerization of mutant SOD1 in mitochondria of motoneuronal cells drives mitochondrial damage and cell toxicity. Antioxid Redox Signal 11:1547–58. doi: 10.1089/ars.2009.2545

26. Pesaresi MG, Amori I, Giorgi C, et al. (2011) Mitochondrial redox signalling by p66Shc mediates ALS-like disease through Rac1 inactivation. Hum Mol Genet 20:4196–208. doi: 10.1093/hmg/ddr347

27. Cozzolino M, Ferri A, Ferraro E, et al. (2006) Apaf1 mediates apoptosis and mitochondrial damage induced by mutant human SOD1s typical of familial amyotrophic lateral sclerosis. Neurobiol Dis 21:69–79. doi: 10.1016/j.nbd.2005.06.010

28. Sasaki S, Iwata M (1999) Ultrastructural change of synapses of Betz cells in patients with amyotrophic lateral sclerosis. Neurosci Lett 268:29–32.

29. Menzies FM, Ince PG, Shaw PJ (2002) Mitochondrial involvement in amyotrophic lateral sclerosis. Neurochem Int 40:543–51.

30. Martin LJ (2011) Mitochondrial pathobiology in ALS. J Bioenerg Biomembr 43:569–79. doi: 10.1007/s10863-011-9395-y

31. Coussee E, De Smet P, Bogaert E, et al. (2011) G37R SOD1 mutant alters mitochondrial complex I activity, Ca(2+) uptake and ATP production. Cell Calcium 49:217–25. doi: 10.1016/j.ceca.2011.02.004

32. Ilieva H, Polymenidou M, Cleveland DW (2009) Non?cell autonomous toxicity in neurodegenerative disorders: ALS and beyond. J Cell Biol 187:761–772. doi: 10.1083/jcb.200908164

33. Haidet-Phillips AM, Hester ME, Miranda CJ, et al. (2011) Astrocytes from familial and sporadic ALS patients are toxic to motor neurons. Nat Biotechnol 29:824–828. doi: 10.1038/nbt.1957

34. Araque A, Parpura V, Sanzgiri RP, Haydon PG (1999) Tripartite synapses: Glia, the unacknowledged partner. Trends Neurosci 22:208–215. doi: 10.1016/S0166-2236(98)01349-6

35. Perea G, Navarrete M, Araque A (2009) Tripartite synapses: astrocytes process and control synaptic information. Trends Neurosci 32:421–431. doi: 10.1016/j.tins.2009.05.001

36. Papouin T, Dunphy J, Tolman M, et al. (2017) Astrocytic control of synaptic function. Philos Trans R Soc B Biol Sci 372:20160154. doi: 10.1098/rstb.2016.0154

37. Allen NJ, Barres BA (2005) Signaling between glia and neurons: focus on synaptic plasticity. Curr Opin Neurobiol 15:542–8. doi: 10.1016/j.conb.2005.08.006

38. Bilsland LG, Nirmalananthan N, Yip J, et al. (2008) Expression of mutant SOD1 ^{G93A} in astrocytes induces functional deficits in motoneuron mitochondria. J Neurochem 107:1271–1283. doi: 10.1111/j.1471-4159.2008.05699.x

39. Nagai M, Re DB, Nagata T, et al. (2007) Astrocytes expressing ALS-linked mutated SOD1 release factors selectively toxic to motor neurons. Nat Neurosci 10:615–622. doi: 10.1038/nn1876

40. Cassina P, Cassina A, Pehar M, et al. (2008) Mitochondrial Dysfunction in SOD1G93A-Bearing Astrocytes Promotes Motor Neuron Degeneration: Prevention by Mitochondrial-

Targeted Antioxidants. J Neurosci 28:4115–4122. doi: 10.1523/JNEUROSCI.5308-07.2008

41. Raiteri L, Stigliani S, Zappettini S, et al. (2004) Excessive and precocious glutamate release in a mouse model of amyotrophic lateral sclerosis. Neuropharmacology 46:782–792. doi: 10.1016/j.neuropharm.2003.11.025

42. Raiteri L, Zappettini S, Stigliani S, et al. (2005) Glutamate Release Induced by Activation of Glycine and GABA Transporters in Spinal Cord is Enhanced in a Mouse Model of Amyotrophic Lateral Sclerosis. Neurotoxicology 26:883–892. doi: 10.1016/j.neuro.2005.01.015

43. Giribaldi F, Milanese M, Bonifacino T, et al. (2013) Group I metabotropic glutamate autoreceptors induce abnormal glutamate exocytosis in a mouse model of amyotrophic lateral sclerosis. Neuropharmacology 66:253–263. doi: 10.1016/j.neuropharm.2012.05.018

44. Milanese M, Zappettini S, Onofri F, et al. (2011) Abnormal exocytotic release of glutamate in a mouse model of amyotrophic lateral sclerosis. J Neurochem 116:1028–1042. doi: 10.1111/j.1471-4159.2010.07155.x

45. Bonifacino T, Musazzi L, Milanese M, et al. (2016) Altered mechanisms underlying the abnormal glutamate release in amyotrophic lateral sclerosis at a pre-symptomatic stage of the disease. Neurobiol Dis 95:122–133. doi: 10.1016/j.nbd.2016.07.011

46. Milanese M, Bonifacino T, Fedele E, et al. (2015) Exocytosis regulates trafficking of GABA and glycine heterotransporters in spinal cord glutamatergic synapses: a mechanism for the excessive heterotransporter-induced release of glutamate in experimental amyotrophic lateral sclerosis. Neurobiol Dis 74:314–324. doi: 10.1016/j.nbd.2014.12.004

47. Milanese M, Zappettini S, Jacchetti E, et al. (2010) *In vitro* activation of GAT1 transporters expressed in spinal cord gliosomes stimulates glutamate release that is abnormally elevated in the SOD1/G93A(+) mouse model of amyotrophic lateral sclerosis. J Neurochem 113:489–501. doi: 10.1111/j.1471-4159.2010.06628.x

48. Whittaker VP (1993) Thirty years of synaptosome research. J Neurocytol 22:735–42.

49. Raiteri M (1983) Synaptosomes as a tool in the development of new neuroactive drugs. Rev Pure Appl Pharmacol Sci 4:65–109.

50. Nakamura Y, Iga K, Shibata T, et al. (1993) Glial plasmalemmal vesicles: a subcellular fraction from rat hippocampal homogenate distinct from synaptosomes. Glia 9:48–56. doi: 10.1002/glia.440090107

51. Stigliani S, Zappettini S, Raiteri L, et al. (2006) Glia re-sealed particles freshly prepared from adult rat brain are competent for exocytotic release of glutamate. J Neurochem 96:656–68. doi: 10.1111/j.1471-4159.2005.03631.x

52. Carney KE, Milanese M, Van Nierop P, et al. (2014) Proteomic analysis of gliosomes from mouse brain: Identification and investigation of glial membrane proteins. J Proteome Res 13:5918–5927. doi: 10.1021/pr500829z

53. Gurney ME, Pu H, Chiu AY, et al. (1994) Motor neuron degeneration in mice that express a human Cu,Zn superoxide dismutase mutation. Science 264:1772–5.

54. Bonifacino T, Cattaneo L, Gallia E, et al. (2017) In-vivo effects of knocking-down metabotropic glutamate receptor 5 in the SOD1 G93A mouse model of amyotrophic lateral sclerosis. Neuropharmacology 123:433–445. doi: 10.1016/j.neuropharm.2017.06.020

55. Bradford MM (1976) A rapid and sensitive method for the quantitation of microgram quantities of protein utilizing the principle of protein-dye binding. Anal Biochem 72:248–254.

56. Cappelli E, Cuccarolo P, Stroppiana G, et al. (2017) Defects in mitochondrial energetic function compels Fanconi Anemia cells to glycolytic metabolism. BBA - Mol Basis Dis. doi: 10.1016/j.bbadis.2017.03.008

57. Ravera S, Panfoli I, Calzia D, et al. (2009) Evidence for aerobic ATP synthesis in isolated myelin vesicles. Int J Biochem Cell Biol 41:1581–1591.

58. Ravera S, Panfoli I, Aluigi MG, et al. (2011) Characterization of Myelin Sheath F(o)F(1)-ATP synthase and its regulation by IF(1). Cell Biochem Biophys 59:63–70.

59. Ravera S, Bartolucci M, Cuccarolo P, et al. (2015) Oxidative stress in myelin sheath: The other face of the extramitochondrial oxidative phosphorylation ability. Free Radic Res 49:1–36. doi: 10.3109/10715762.2015.1050962

60. Kirkinezos IG, Bacman SR, Hernandez D, et al. (2005) Cytochrome c Association with the Inner Mitochondrial Membrane Is Impaired in the CNS of G93A-SOD1 Mice. J Neurosci 25:164–172. doi: 10.1523/JNEUROSCI.3829-04.2005

61. Boyer PD (2002) A research journey with ATP synthase. J Biol Chem 277:39045–39061.

62. Collard J-F, Côté F, Julien J-P (1995) Defective axonal transport in a transgenic mouse model of amyotrophic lateral sclerosis. Nature 375:61–64. doi: 10.1038/375061a0

63. Williamson TL, Cleveland DW (1999) Slowing of axonal transport is a very early event in the toxicity of ALS-linked SOD1 mutants to motor neurons. Nat Neurosci 2:50–6. doi: 10.1038/4553

64. Pfanner N, Meijer M (1997) Mitochondrial biogenesis: The Tom and Tim machine. Curr Biol 7:R100–R103. doi: 10.1016/S0960-9822(06)00048-0

65. Capaldi RA, Malatesta F, Darley-Usmar VM (1983) Structure of cytochrome c oxidase. Biochim Biophys Acta - Rev Bioenerg 726:135–148. doi: 10.1016/0304-4173(83)90003-4

66. Cadenas E, Davies KJA (2000) Mitochondrial free radical generation, oxidative stress, and aging. Free Radic Biol Med 29:222–230. doi: 10.1016/S0891-5849(00)00317-8

67. Sasaki S, Iwata M (2007) Mitochondrial Alterations in the Spinal Cord of Patients With Sporadic Amyotrophic Lateral Sclerosis. J Neuropathol Exp Neurol 66:10–16. doi: 10.1097/nen.0b013e31802c396b

68. Ghijsen WEJM, Leenders AGM, Lopes da Silva FH (2003) Regulation of vesicle traffic and neurotransmitter release in isolated nerve terminals. Neurochem Res 28:1443–52.

69. Ferraiuolo L, Higginbottom A, Heath PR, et al. (2011) Dysregulation of astrocyte-motoneuron cross-talk in mutant superoxide dismutase 1-related amyotrophic lateral sclerosis. Brain 134:2627–41. doi: 10.1093/brain/awr193

70. Paluzzi S, Alloisio S, Zappettini S, et al. (2007) Adult astroglia is competent for Na^+/Ca^{2+} exchanger-operated exocytotic glutamate release triggered by mild depolarization. J Neurochem 103:1196–1207. doi: 10.1111/j.1471-4159.2007.04826.x

71. Tsujimoto Y, Nakagawa T, Shimizu S (2006) Mitochondrial membrane permeability transition and cell death. Biochim Biophys Acta - Bioenerg 1757:1297–1300. doi: 10.1016/j.bbabio.2006.03.017

72. Quintanilla RA, Jin YN, von Bernhardi R, Johnson GVW (2013) Mitochondrial permeability transition pore induces mitochondria injury in Huntington disease. Mol Neurodegener 8:45. doi: 10.1186/1750-1326-8-45

73. Tiwari BS, Belenghi B, Levine A (2002) Oxidative stress increased respiration and generation of reactive oxygen species, resulting in ATP depletion, opening of mitochondrial permeability transition, and programmed cell death. Plant Physiol 128:1271–81. doi: 10.1104/pp.010999

74. Dai D-F, Chiao YA, Marcinek DJ, et al. (2014) Mitochondrial oxidative stress in aging and healthspan. Longev Heal 3:6. doi: 10.1186/2046-2395-3-6

75. Chen Q, Vazquez EJ, Moghaddas S, et al. (2003) Production of reactive oxygen species by mitochondria: central role of complex III. J Biol Chem 278:36027–36031. doi: 10.1074/jbc.M304854200

76. Lenaz G (2001) The mitochondrial production of reactive oxygen species: mechanisms and implications in human pathology. IUBMB Life 52:159–64. doi: 10.1080/15216540152845957

77. Fang C, Bourdette D, Banker G (2012) Oxidative stress inhibits axonal transport: implications for neurodegenerative diseases. Mol Neurodegener 7:29. doi: 10.1186/1750-1326-7-29

78. Boillée S, Vande Velde C, Cleveland DWW (2006) ALS: A Disease of Motor Neurons and Their Nonneuronal Neighbors. Neuron 52:39–59. doi: 10.1016/j.neuron.2006.09.018

79. Yamanaka K, Chun SJ, Boillee S, et al. (2008) Astrocytes as determinants of disease progression in inherited amyotrophic lateral sclerosis. Nat Neurosci 11:251–253. doi: 10.1038/nn2047

FIGURE LEGENDS

Figure 1. Energy status in spinal cord synaptosomes and gliosomes from *wtSOD1* and *SOD1^{G93A}* mice

ATP/AMP ratio, as a marker of the energy status, was measured in synaptosomes and in gliosomes isolated from spinal cord, cortex, hippocampus and cerebellum of *wtSOD1* and *SOD1^{G93A}* mice at different stage of the disease (30, 60, 90 and 120 days of life). Panels A and B report the energy status of spinal cord synaptosomes and gliosomes. Panels C and D report the energy status of cortex, hippocampus and cerebellum synaptosomes and gliosomes. Data are the expressed as the ratio between ATP and AMP concentrations and are the mean ± s.e.m of 4 independent experiments run in triplicate. * $p<0.05$ and ** $p<0.001$ vs *wtSOD1* mice (two-way ANOVA followed by Bonferroni post-hoc test).

Figure 2. Oxygen consumption in spinal cord synaptosomes and gliosomes from *wtSOD1* and *SOD1^{G93A}* mice

Oxygen consumption was measured in synaptosomes and gliosomes isolated from the spinal cord of *wtSOD1* and *SOD1^{G93A}* mice at different stage of the disease (30, 60, 90 and 120 days of life). Panels A and C report the synaptosomal oxygen consumption induced, respectively, by pyruvate + malate, that activate Complexes I, III and IV pathways or by succinate, that activates Complexes II, III and IV pathways. Panels B and D report the same experiments in gliosomes. Data are expressed as nmol of oxygen consumption per min per mg protein and are the mean ± s.e.m of 4 independent experiments run in triplicate. * $p<0.01$ and ** $p<0.001$ vs *wtSOD1* mice; # $p<0.01$ and ## $p<0.001$ vs. 30 days-old *wtSOD1* mice (two-way ANOVA followed by Bonferroni post-hoc test).

Figure 3. Activity of respiratory complexes in spinal cord synaptosomes and gliosomes purified from *wtSOD1* and *SOD1^{G93A}* mice

The activity of the respiratory complexes was measured in synaptosomes and gliosomes isolated from the spinal cord of *wtSOD1* and *SOD1^{G93A}* mice at different stage of the disease (30, 60, 90 and 120 days of life). The activity of NADH ubiquinone oxidoreductase (Complex I; panels A and B), of succinic dehydrogenase (Complex II; panels C and D), of cytochrome c reductase (Complex III; panels E and F), or of cytochrome c oxidase (Complex IV; panels G and H) in synaptosomes and gliosomes is reported. Data are expressed as international milliunits (mUI) of each respiratory complex per mg of protein and are the mean ± s.e.m. of 4 independent experiments run in triplicate. * $p<0.05$ and ** $p<0.001$ vs *wtSOD1* mice; # $p<0.001$ vs. 30 days-old *wtSOD1* mice (two-way ANOVA followed by Bonferroni post-hoc test).

Figure 4. ATP production in spinal cord synaptosomes and gliosomes from *wtSOD1* and *SOD1^{G93A}*mice

ATP synthesis, as a marker of F_1Fo-ATP synthase activity, was measured in synaptosomes and gliosomes isolated from spinal cord of *wtSOD1* and *SOD1^{G93A}* mice at different stage of the disease (30, 60, 90 and 120 days of life). ATP synthesis induced by pyruvate + malate, that activate Complex I, III and IV pathways in synaptosomes (panel A) and gliosomes (panel B) or by succinate, that activates Complex II, III and IV pathways in synaptosomes (panel C) and gliosomes (panel D) is reported. Data are expressed as nmol of ATP produced per min per mg of protein and are the mean ± s.e.m of 4 independent experiments run in triplicate. * $p<0.01$ and **$p<0.001$ vs *wtSOD1* mice; # $p<0.001$ vs *wtSOD1* mice at 30 days-old (two-way ANOVA followed by Bonferroni post-hoc test).

Figure 5. Mitochondrial content and expression of F_1F_o-ATP synthase β subunit, MT-CO2 and TIM in spinal cord of *wtSOD1* and *SOD1^{G93A}* mice

The morphology of mitochondria (indicated with *m*) in synaptosomes purified from spinal cord of *wt*SOD1 and SOD1^{G93A} mice (120 days of age) was evaluated by electron microscopy (A). All data are representative of 3 independent experiments run in triplicate. Scale bar = 200 nm.
The content of mitochondria in spinal cord synaptosomes wtSOD1 and SOD1^{G93A} mice (120 days of age) was evaluated as the ratio of mitochondria number/synaptosomes number (B) and as the ratio of the surface occupied by mitochondria compared with the total surface of synaptosomes (C).

The expression of mitochondrial import inner membrane translocase (TIM), the β subunit of F_1F_o-ATP synthase and MT-CO2 (a subunit of complex IV) was evaluated in *SOD1^{G93A}* mouse spinal cord synaptosomes at different stage of the disease (30, 60, 90 and 120 days of life). Representative blots (D) and densitometric analyses (E, F and G) are shown. Data are expressed as relative signal densities for *SOD1^{G93A}* vs *wtSOD1* mice and are the means ± s.e.m of 4 independent experiments run in triplicate. The signal densities were normalized for GAPDH.

Figure 6. Evaluation of lipid peroxidation in spinal cord synaptosomes and gliosomes purified from *wtSOD1* and *SOD1^{G93A}* mice

Malondialdehyde (MDA), a marker of lipid peroxidation, was measured in synaptosomes (A) and gliosomes (B) isolated from the spinal cord of *wtSOD1* and *SOD1^{G93A}* mice at different stage of the disease (30, 60, 90 and 120 days of life). Data are expressed as μmol of MDA per mg of protein and are the mean ± s.e.m. of 4 independent experiments run in triplicate. * $p<0.01$ and ** $p<0.001$ vs *wtSOD1* mice; # $p<0.001$ vs. 30 days-old *wtSOD1* mice (two-way ANOVA followed by Bonferroni post-hoc test).

Figure 1

Click here to download Figure Ravera et al Figure 1_bioenergGS.tif

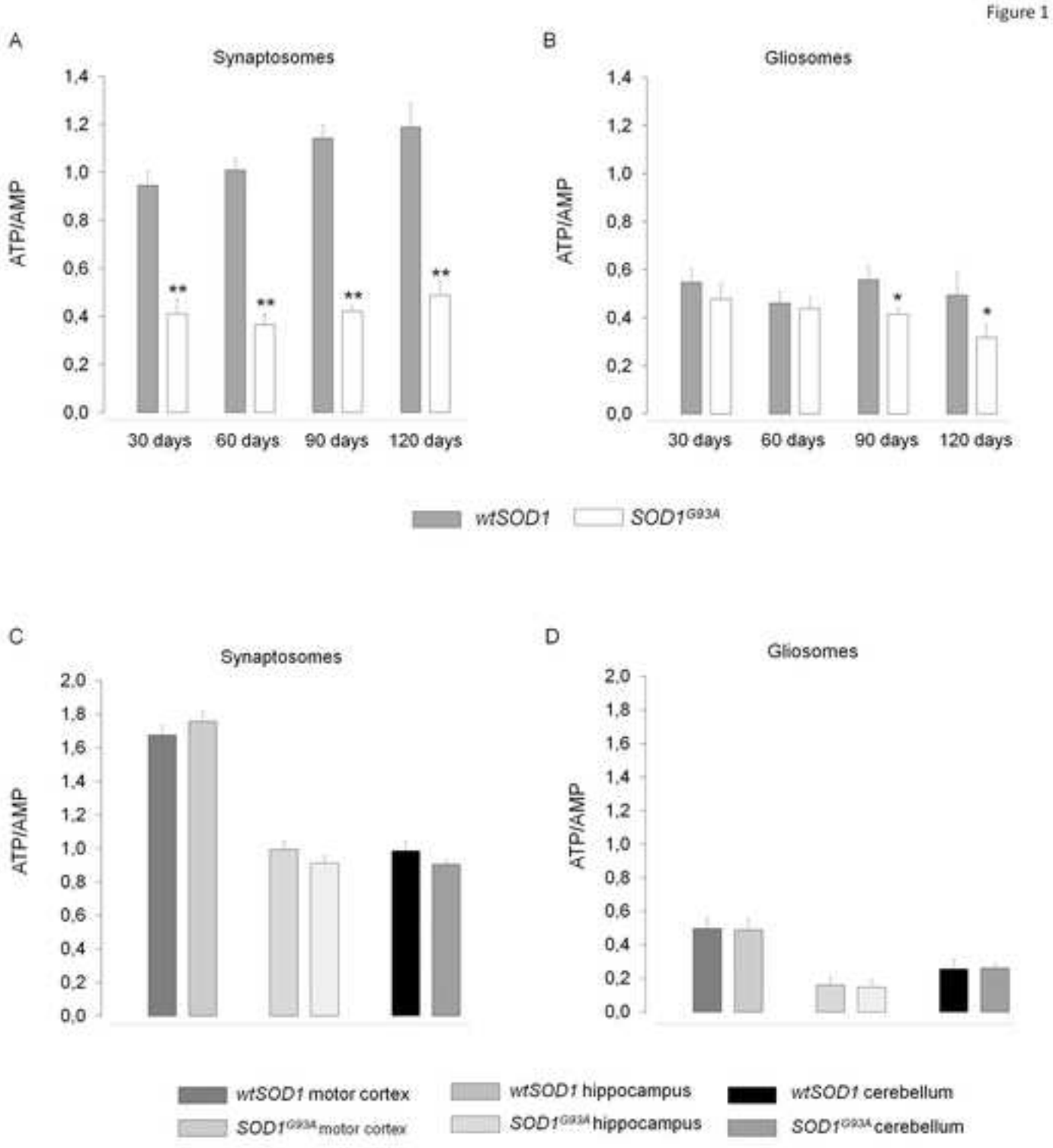

Figure 2

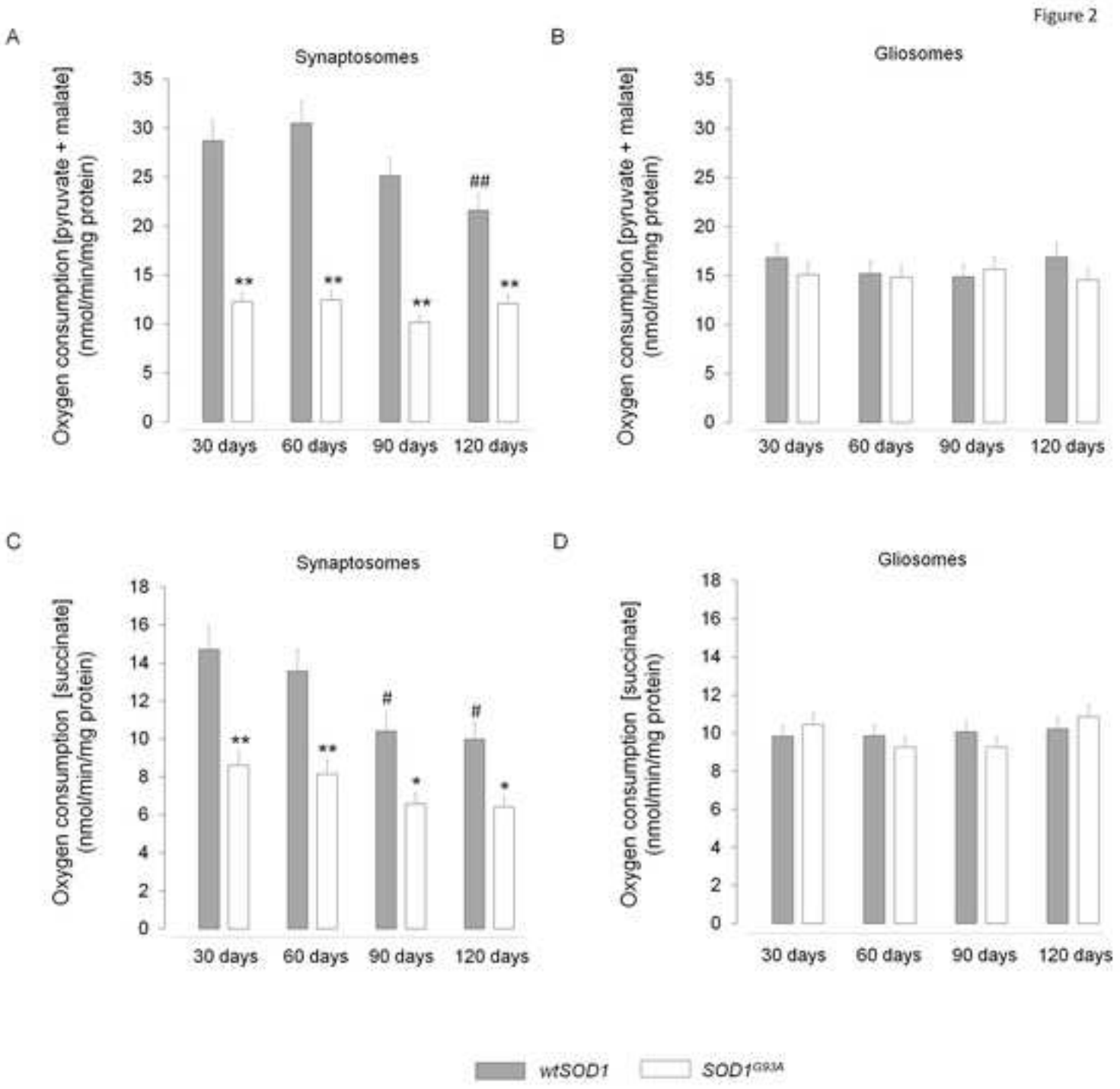

Figure 3

Click here to download Figure Ravera et al Figure 3_bioenergGS.tif

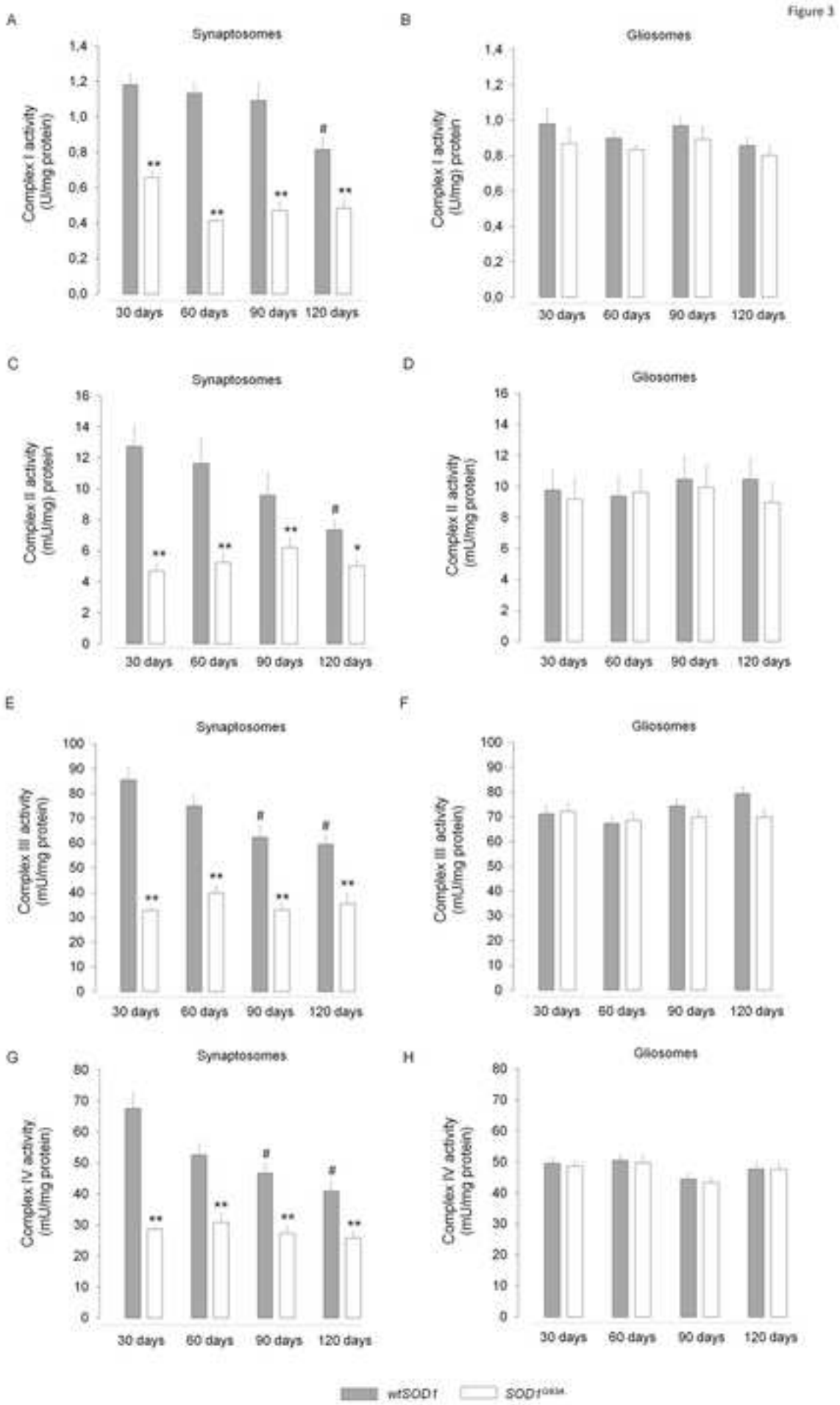

Figure 4

Click here to download Figure Ravera et al Figure 4_bioenergGS.tif

Figure 4

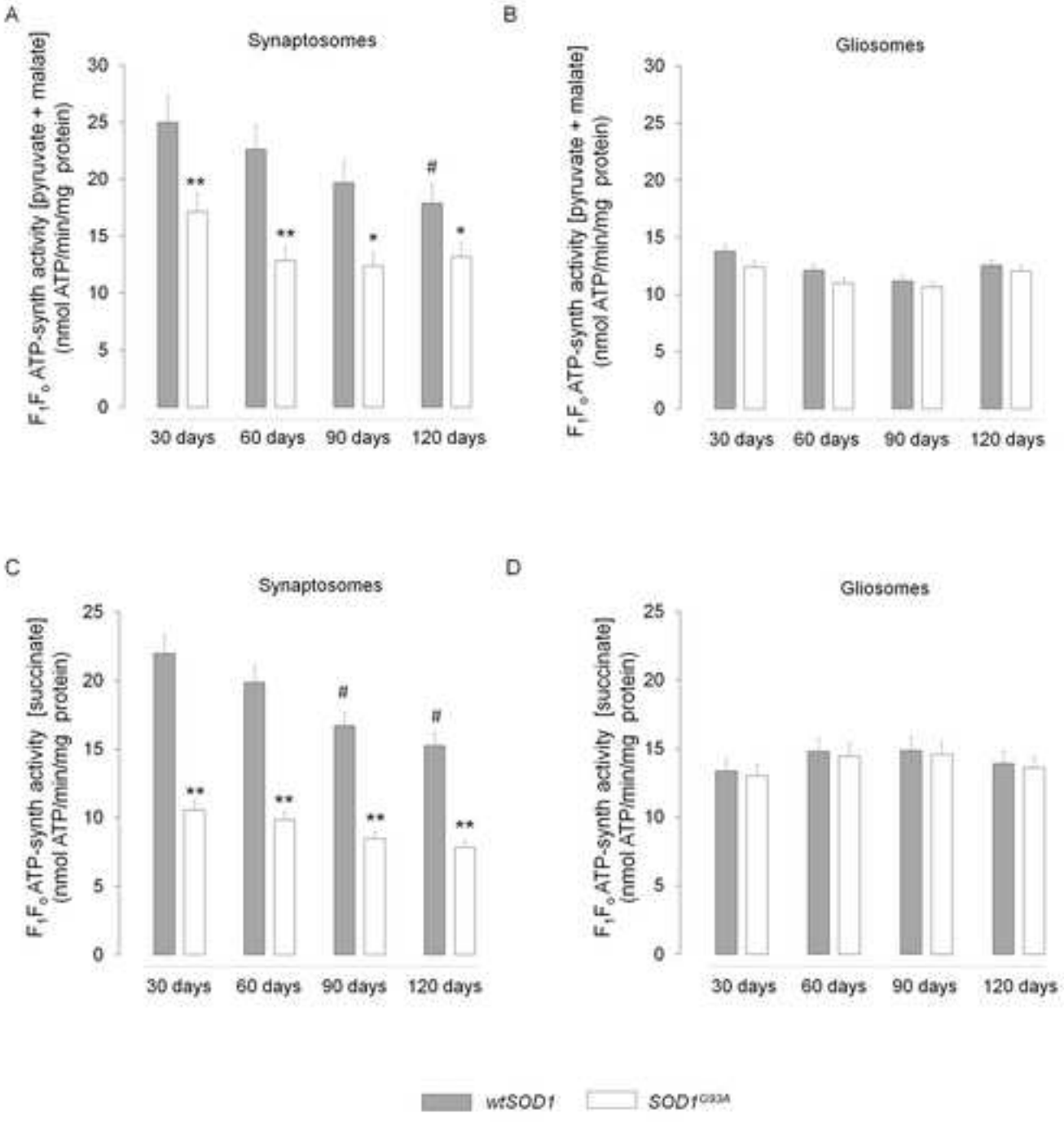

Figure 5

Click here to download Figure Ravera et al Figure 5_bioenergGS.tif

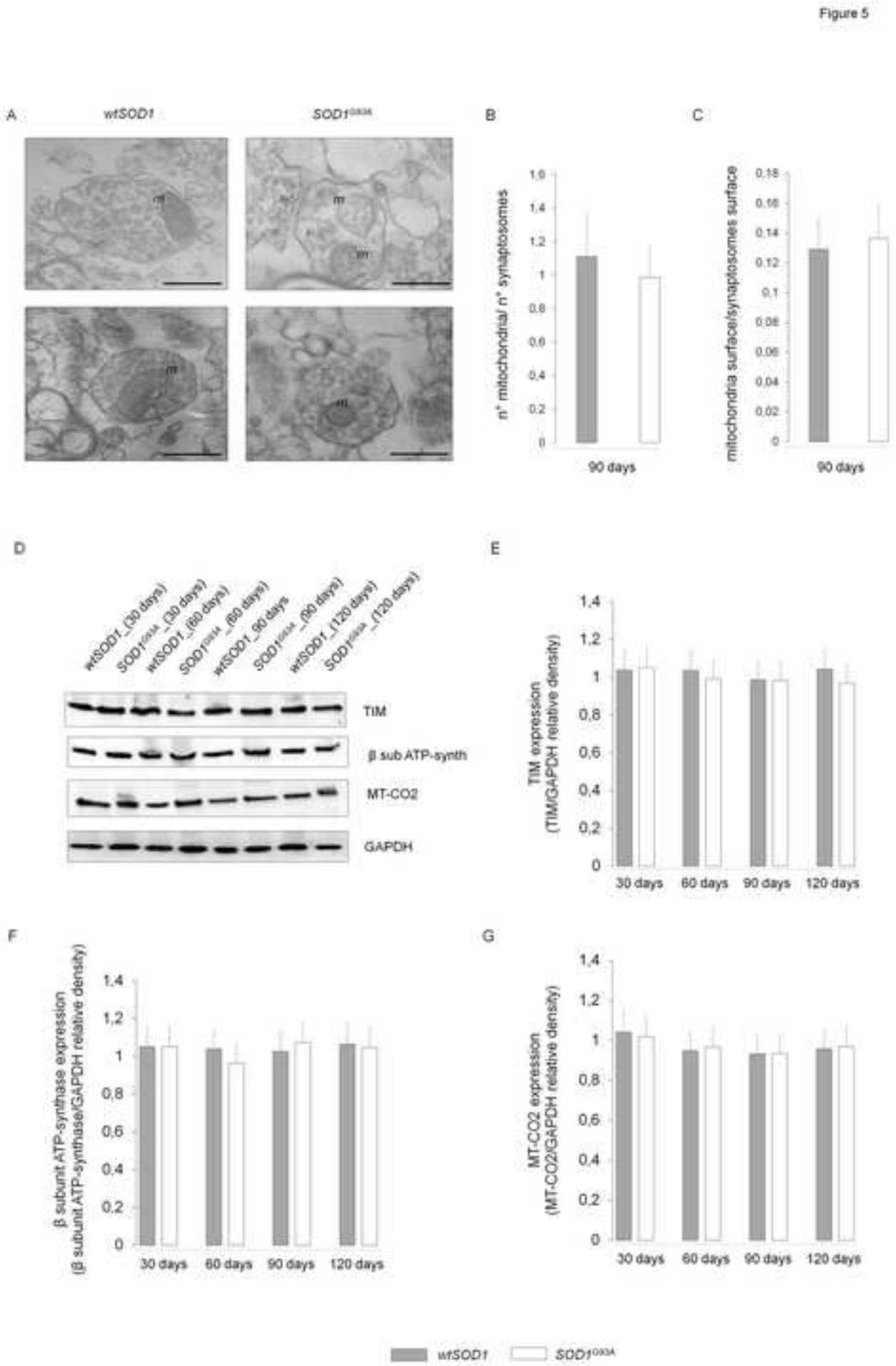

Figure 6